



Article

# Enhancing Tin Dioxide Anode Performance by Narrowing the Potential Range and Optimizing Electrolytes

Jose Fernando Florez Gomez <sup>1</sup>, Fernando Camacho Domenech <sup>2</sup>, Songyang Chang <sup>3</sup> , Valerio Dorvilien <sup>1</sup>, Nischal Oli <sup>1</sup> , Brad R. Weiner <sup>3</sup> , Gerardo Morell <sup>1,\*</sup> and Xianyong Wu <sup>3,\*</sup>

<sup>1</sup> Department of Physics, University of Puerto Rico, Rio Piedras Campus, San Juan, PR 00925, USA; jose.florez@upr.edu (J.F.F.G.); valerio.dorvilien@upr.edu (V.D.); nischal.ol@upr.edu (N.O.)

<sup>2</sup> Department of Chemical Engineering, University of Puerto Rico, Mayaguez Campus, Mayaguez, PR 00680, USA; fernando.camacho1@upr.edu

<sup>3</sup> Department of Chemistry, University of Puerto Rico, Rio Piedras Campus, San Juan, PR 00925, USA; songyang.chang@upr.edu (S.C.); brad.weiner@upr.edu (B.R.W.)

\* Correspondence: gerardo.morell@upr.edu (G.M.); xianyong.wu@upr.edu (X.W.)

**Abstract:** Tin dioxide ( $\text{SnO}_2$ ) is a low-cost and high-capacity anode material for lithium-ion batteries, but the fast capacity fading significantly limits its practical applications. Current research efforts have focused on preparing sophisticated composite structures or optimizing functional binders, both of which increase material manufacturing costs. Herein, we utilize pristine and commercially available  $\text{SnO}_2$  nanopowders and enhance their cycling performance by simply narrowing the potential range and optimizing electrolytes. Specifically, a narrower potential range (0–1 V) mitigates the capacity fading associated with the conversion reaction, whereas an ether-based electrolyte further suppresses the volume expansion related to the alloy reaction. Consequently, this  $\text{SnO}_2$  anode delivers a promising battery performance, with a high capacity of  $\sim 650 \text{ mAh g}^{-1}$  and stable cycling for 100 cycles. Our work provides an alternative approach to developing high-capacity and long-cycling metal oxide anode materials.



**Citation:** Florez Gomez, J.F.; Domenech, F.C.; Chang, S.; Dorvilien, V.; Oli, N.; Weiner, B.R.; Morell, G.; Wu, X. Enhancing Tin Dioxide Anode Performance by Narrowing the Potential Range and Optimizing Electrolytes. *Batteries* **2024**, *10*, 334. <https://doi.org/10.3390/batteries10090334>

Academic Editor: Marco Giorgetti

Received: 29 July 2024

Revised: 12 September 2024

Accepted: 19 September 2024

Published: 21 September 2024



**Copyright:** © 2024 by the authors. Licensee MDPI, Basel, Switzerland. This article is an open access article distributed under the terms and conditions of the Creative Commons Attribution (CC BY) license (<https://creativecommons.org/licenses/by/4.0/>).

## 1. Introduction

Li-ion batteries (LIBs) are considered one of the most important inventions that have transformed our way of electric energy use, ranging from portable electronics (cellphones, laptops) to electric vehicles (EVs) [1,2]. LIBs work on a classic “rocking-chair” battery mechanism, featuring a layered metal oxide cathode and a layered graphite anode [3]. However, the moderate capacity in the graphite anode ( $\sim 370 \text{ mAh g}^{-1}$ ) restricts the LIB energy density to  $150\text{--}200 \text{ Wh kg}^{-1}$ , which cannot satisfy the growing demand for high-energy applications, especially long-range EVs [4,5]. Moreover, the  $\text{Li}^+$  intercalation potential in the graphite (0.1 V) is close to that of Li metal plating, which limits the fast-charging capability in LIB full cells [6–8]. Otherwise, Li plating will take place on the graphite surface, leading to safety concerns. Therefore, it is of vital importance to develop an alternative anode material with higher capacities and suitable potentials.

Alloy-based materials are promising choices for high-energy batteries [9–13], due to their high capacity ( $600\text{--}2800 \text{ mAh g}^{-1}$ ) and feasible reaction potentials (0.2–1.0 V). Among various alloy-based materials, tin dioxide ( $\text{SnO}_2$ ) stands out as a promising candidate [14–16]. Firstly, it exhibits a high theoretical capacity of  $1491 \text{ mAh g}^{-1}$  based on eight-electron reactions, which is much higher than that of graphite ( $372 \text{ mAh g}^{-1}$ ) and  $\text{Li}_4\text{Ti}_5\text{O}_{12}$  ( $175 \text{ mAh g}^{-1}$ ). In the 1–2 V potential range, it first reacts with  $4 \text{ Li}^+$  and converts to lithium oxide ( $\text{Li}_2\text{O}$ ) and tin metal, leading to a good capacity of  $711 \text{ mAh g}^{-1}$ . Subsequently, in the 0–1 V range, the Sn metal further reacts with  $4.4 \text{ Li}^+$  ions and transforms into a  $\text{Li}_{4.4}\text{Sn}$  alloy, resulting in an extra capacity of  $783 \text{ mAh g}^{-1}$ . Secondly, this material has a

desirable reaction potential with an average potential of ~0.4 V vs. Li/Li<sup>+</sup>, which is higher than graphite (~0.1 V) but much lower than Li<sub>4</sub>Ti<sub>5</sub>O<sub>12</sub> (~1.5 V). Therefore, it effectively avoids the Li metal plating issue on the graphite anode under abnormal conditions and ensures a high voltage output in the full-cell configuration. Thirdly, SnO<sub>2</sub> is a low-toxicity material with relatively low cost and easy synthesis. Lastly, SnO<sub>2</sub> contains the tin metal element, leading to good electric conductivity. This is an advantage over silicon-based anodes, which exhibit moderate electric conductivity. Based on these considerations, SnO<sub>2</sub> has been extensively studied for Li-ion batteries in the past two decades [17–19]. However, this anode material has yet to be commercialized, due to its underlying working mechanisms and substantial challenges. Firstly, the conversion reaction in the high-voltage range (1–2 V) is associated with two-phase solid–solid contact (Sn + Li<sub>2</sub>O), which shows intrinsically low reversibility and results in fast capacity fading. Secondly, this material encounters an overall large volume change ratio, which damages the solid–electrolyte interphase (SEI), further contributing to the capacity fading.

To address these issues, researchers have proposed the use of nano-sizing or carbon coating to enhance battery performance [20,21]. For instance, Hong et al. demonstrated a SnO<sub>2</sub>-based structure embedded in a hierarchical porous carbon framework and further coated it in a nitrogen-doped carbon layer, which showed a long-term cycling of 500 cycles with ~730 mAhg<sup>-1</sup> capacity retention [22]. As another example, Wang et al. fabricated ultrafine SnO<sub>2</sub> nanoparticles anchored in carbon framework microbelts, which delivered a high capacity of 925 mAhg<sup>-1</sup> after 250 cycles [23]. However, it is noted that the research innovation is mostly on materials instead of the potential range or electrolytes. Therefore, there is a knowledge gap on how the potential range and electrolyte properties affect SnO<sub>2</sub> anode performance.

Herein, we used a simple and effective method to enhance SnO<sub>2</sub> performance by narrowing the working potential and optimizing the electrolyte. We find that the capacity fading mostly comes from the conversion reaction (1–2 V region) in the conventional carbonate electrolyte, and a higher capacity retention can be achieved in a narrower range of 0–1 V. Moreover, replacing the carbonate electrolyte with an ether electrolyte reduces side reactions and alleviates electrode pulverization, which further enhances the capacity and cycling performance. Consequently, this pristine and commercially available SnO<sub>2</sub> material exhibited a high capacity of 650 mAh g<sup>-1</sup>, a good rate capability of 1000 mA g<sup>-1</sup>, and a stable cycling performance of 100 cycles (89% retention).

## 2. Materials and Methods

### 2.1. Electrode Preparation

Tin (IV) oxide was purchased from Sigma-Aldrich (St. Louis, MO, USA) (99.9% metal basis) without further treatment. To make the electrode, SnO<sub>2</sub> was ground with Super P carbon and sodium-carboxymethyl cellulose binder (Na-CMC, MTI Corporation, Richmond, CA, USA, 99.5% purity) in a weight ratio of 7:2:1 into a homogeneous slurry, which was coated on the copper foil substrate (9 μm thickness, MTI Corporation, Richmond, CA, USA, battery grade). The electrode was dried at room temperature overnight. The electrodes were punched into circular shapes (1 cm in diameter) and vacuum-dried before being transferred into the glovebox. The active mass loading per electrode is ~1.8 mg cm<sup>-2</sup>.

### 2.2. Coin Cell Assembly

The SnO<sub>2</sub> electrode was transferred to a glovebox (VigorTech, Houston, TX, USA) to assemble 2032-type coin cells, using a lithium foil as the counter and reference electrode and a polypropylene ethylene PPE (Celgard, Charlotte, SC, USA) separator. Two different electrolytes were used to compare the electrochemical performance. We prepared 2 M of LiPF<sub>6</sub> in a 1:1 (*v/v*) ratio of tetrahydrofuran (THF, Sigma Aldrich, St. Louis, MI, USA, ≥99.9%) and 2-methyltetrahydrofuran (m-THF, Sigma Aldrich, ≥99.5%), which is referred to in this work as the ether-based electrolyte. Meanwhile, 1 M of LiPF<sub>6</sub> in a 1:1 ratio of ethylene carbonate and diethyl carbonate (EC/DEC, Sigma Aldrich, battery grade) with

10% of fluoroethylene carbonate (FEC, Sigma Aldrich,  $\geq 99.0\%$ ) is referred to as the carbonate electrolyte. Both electrolytes were prepared by dissolving salt into the solvent mixtures in their respective ratios inside an Ar-filled glovebox.

### 2.3. Physical and Electrochemical Characterization

XRD results were obtained on the Rigaku SuperNova (HyPix3000 X-ray detector, CuK $\alpha$  radiation source  $\lambda = 1.5406 \text{ \AA}$ ) (Rigaku Corporation, Tokyo, Japan). SEM images and EDS mapping were recorded using a field emission scanning electron microscope (SEM, JEOL, JSM-6480LV) (JEOL, Akishima, Japan). GCD, rate, and cycling performance were tested on the Landt battery tester (CT3002AU) (Landt Instruments, Guangdong, China). EIS analysis was performed on the Biologic potentiostat (SP-150) (BioLogic, Seyssinet-Pariset, France).

## 3. Results and Discussion

In this work, we aim to reveal the effect of the potential range and electrolyte on SnO<sub>2</sub> performance. Therefore, a commercially available SnO<sub>2</sub> material was directly used without further treatment. This material was simply ground with carbon in a mortar for 15–20 min and then made into electrodes for use, which can reduce the material and electrode manufacturing cost. It is noted that this research experience can extend to other types of SnO<sub>2</sub> materials in future studies, which can lead to even better battery performance.

Figure 1a shows the X-ray diffraction (XRD) pattern, where all the diffraction peaks can be attributed to the standard SnO<sub>2</sub> compound (PDF#41-1445). According to the literature [24], it adopts a cassiterite crystal phase with a tetragonal rutile structure (space group: D<sub>4h</sub><sup>14</sup> P4/mnm). There are no extra unidentified peaks, indicating a high chemical purity. The diffraction peaks are somewhat broad, implying a nanometer particle size.

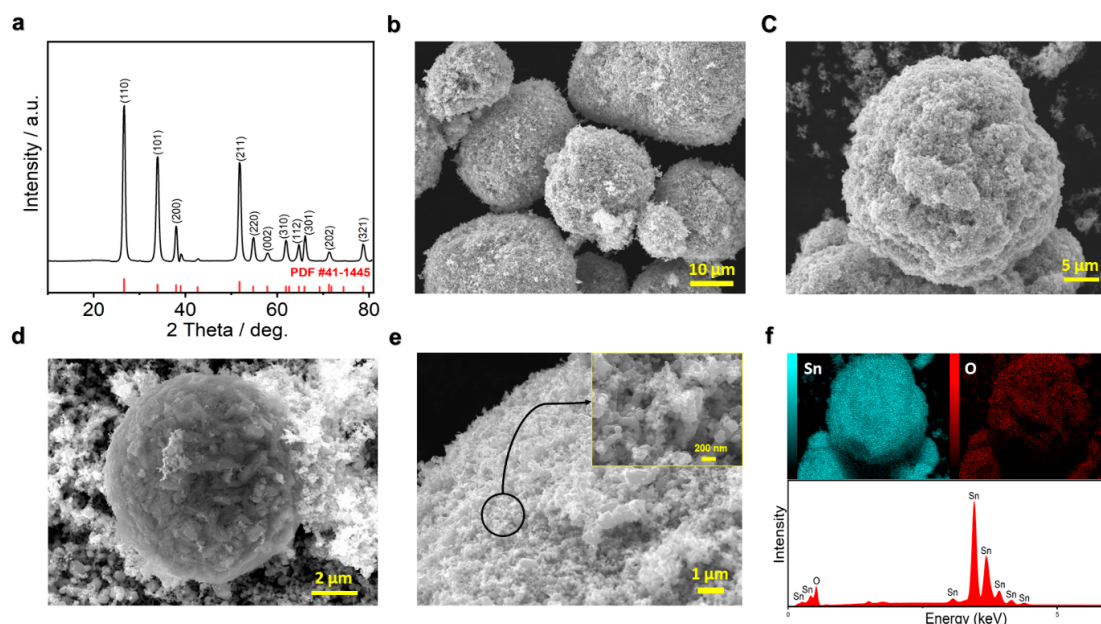


**Figure 1.** Physical characterizations of the SnO<sub>2</sub> material. (a) XRD pattern; (b–e) SEM images at different magnifications; (f) EDS elemental and mapping analysis.

We utilized scanning electron microscopy (SEM) to examine the SnO<sub>2</sub> morphology features. Before grinding, the pristine material exhibits an agglomerated spherical morphology (Figure 1b,c), and the sphere size reaches 30–50  $\mu\text{m}$ . This micro-sized and spherical morphology is beneficial to increase the tap density of electrode materials [25,26], which is a desirable property in Li-ion batteries. Close examination reveals that the agglomerated chunk is composed of many nano-sized SnO<sub>2</sub> sub-particles (Figure 1d,e). These SnO<sub>2</sub> sub-particles are well dispersed, and their particle size is approximately 10–100 nm

(Figure 1e inset). Energy-dispersive spectroscopy (EDS) finds that the Sn and O elements are homogeneously distributed in the sample (Figure 1f), and the atomic ratio is close to 1:2, suggesting the purity of the material.

In most  $\text{SnO}_2$  studies [20,27], a wide potential range of 0–2 V has been utilized, which contributes to a higher capacity, yet at the cost of decreased cycling stability. As a result, obvious capacity fading can be observed even within a few cycles. Herein, we utilized two potential ranges for comparison: 0–2 V and 0–1 V. The battery performance is evaluated in a standard electrolyte of 1 M  $\text{LiPF}_6$ /EC-DEC (1:1 volume ratio, 10% FEC additives).

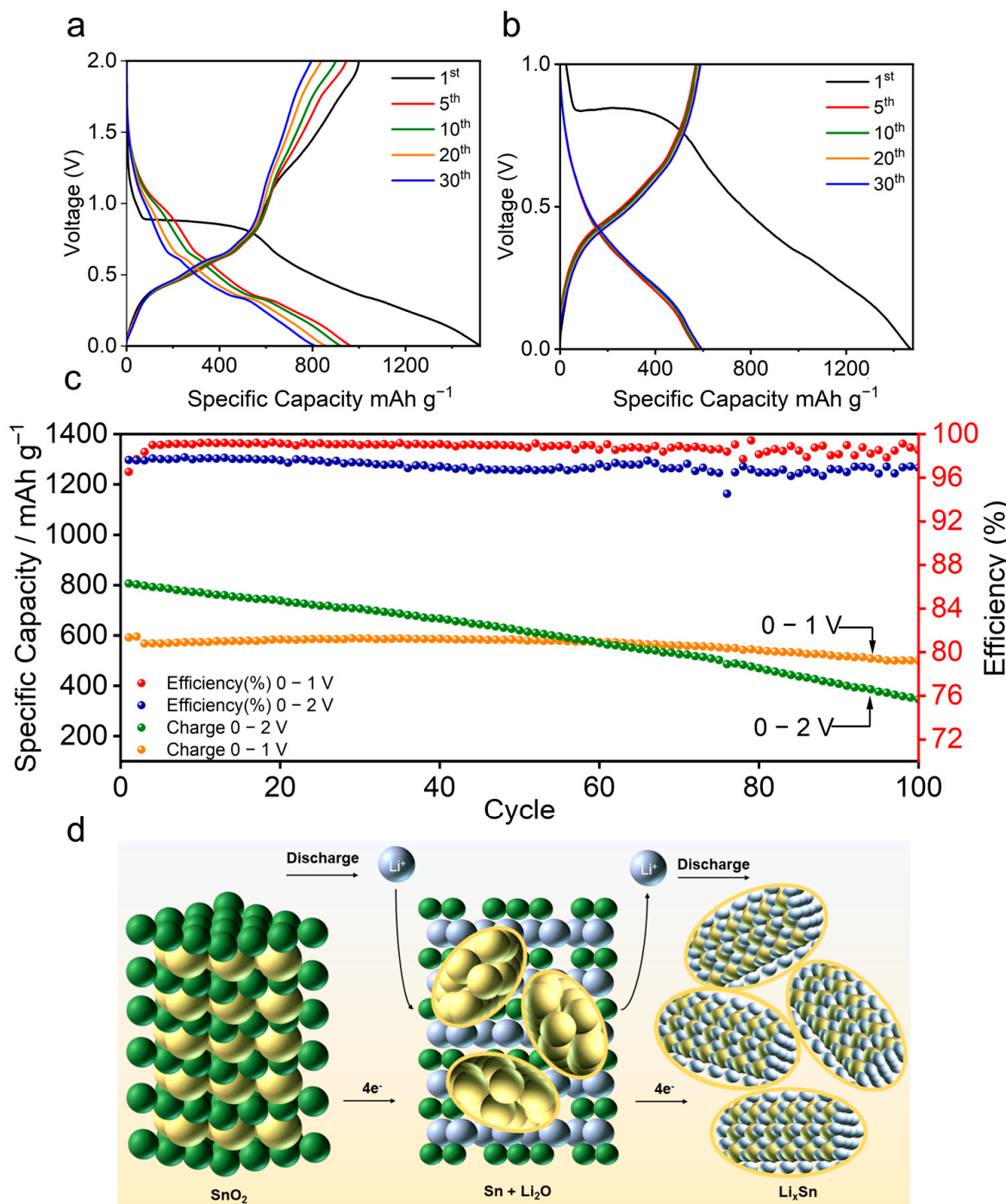
Figure 2a displays galvanostatic charge/discharge (GCD) curves of the  $\text{SnO}_2$  material in the 0–2 V range, wherein the initial discharge/charge capacity is  $1524/999 \text{ mAh g}^{-1}$ , corresponding to a moderate Coulombic efficiency of 65.53%. There is a long discharge plateau at ~0.8 V, and the capacity is not reversible, which is likely due to the carbonate electrolyte decomposition and the SEI formation [28,29]. Although the initial charge capacity is as high as  $\sim 999 \text{ mAh g}^{-1}$ , the charge capacity quickly fades to  $795 \text{ mAh g}^{-1}$  in 30 cycles. Close observation reveals that the capacity fading mostly comes from the 1–2 V range, whereas the 0–1 V region capacity is significantly more stable. This phenomenon motivates us to test the  $\text{SnO}_2$  performance in the 0–1 V range only. As shown in Figure 2b, the  $\text{SnO}_2$  electrode exhibits much-improved and well-overlapped GCD curves, with the capacity stabilized at  $\sim 600 \text{ mAh g}^{-1}$  for 30 cycles without noticeable fading.

Figure 2c shows the capacity and Coulombic efficiency comparison of these two conditions. Despite the lower capacity in the 0–1 V range,  $\text{SnO}_2$  retains a much better capacity retention of 84% over 100 cycles. By contrast, the capacity retention is only 43% in the 0–2 V range. Additionally, the average Coulombic efficiency in the 0–1 V range is 98.2%, which also exceeds that in the 0–2 V range (97.1%). We believe that the  $\text{SnO}_2$  reaction mechanism accounts for its performance difference (Figure 2d) [30,31]. It is well reported that during the initial  $\text{Li}^+$  insertion (1–2 V),  $\text{SnO}_2$  experiences a conversion reaction and forms  $\text{Li}_2\text{O}$  and Sn metal as the intermediate products. Upon further lithiation (0–1 V), the Sn metal further reacts with  $\text{Li}^+$  ions and yields  $\text{Li}_{4.4}\text{Sn}$  alloy, whereas the  $\text{Li}_2\text{O}$  matrix remains unreacted and can partially buffer the volume change. Since the conversion reaction relies on two-phase solid–solid contact ( $\text{Sn} + \text{Li}_2\text{O}$ ), the reaction reversibility is inferior to the subsequent one-phase alloy reaction ( $\text{Li}^+$  ions + Sn). Therefore, when a narrower potential range is used, a much-improved cycling performance can be achieved. This phenomenon also suggests that we can obtain a high-capacity and long-cycling  $\text{SnO}_2$  electrode by sacrificing certain capacities.

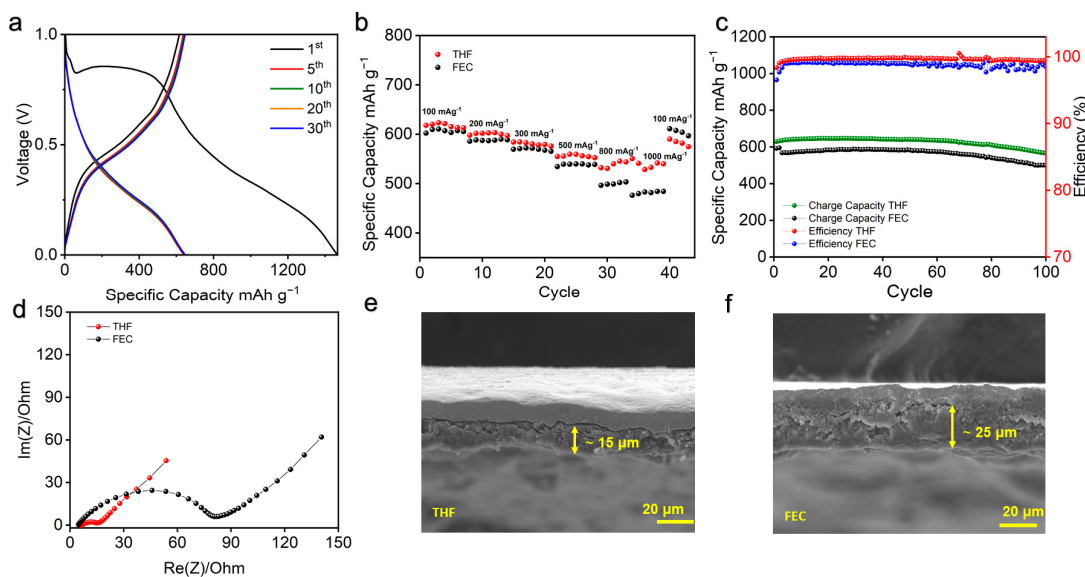
We then explored the electrolyte properties to further enhance the  $\text{SnO}_2$  performance, where two representative electrolytes were selected: the conventional carbonate electrolyte of 1 M  $\text{LiPF}_6$ /EC-DEC + 10% FEC additives and the newly developed ether electrolyte of 1.0 M  $\text{LiPF}_6$ /THF-mTHF. Of note, the ether electrolyte has been reported to induce the formation of lithium fluoride-rich SEI layers [32], which can markedly boost the Li metal and alloy battery performance when used with silicon, tin, and antimony.

Figure 3a provides the GCD curve of  $\text{SnO}_2$  in the ether electrolyte in the 0–1 V range, wherein a representative and well-overlapped charge/discharge curve is obtained. Compared with the carbonate electrolyte, this ether electrolyte leads to a higher charge capacity of  $\sim 650 \text{ mAh g}^{-1}$ . Impressively, the ether electrolyte also renders an improved rate performance. As shown in Figure 3b, the charge capacity is 623, 602, 580, 559, and  $539 \text{ mAh g}^{-1}$  at 100, 200, 300, 500, and  $800 \text{ mA g}^{-1}$  current density, respectively. Even at  $1000 \text{ mA g}^{-1}$ , the charge capacity is still  $528 \text{ mAh g}^{-1}$ , which corresponds to a capacity utilization of ~81%. In stark contrast, the carbonate electrolyte exhibits an overall inferior rate performance, suggesting slower reaction kinetics. Of note, there is a slight capacity increase in Figure 3b at  $800 \text{ mA g}^{-1}$ , which was due to the temperature variation during the battery testing process. In addition, the ether electrolyte results in a better cycling performance. As shown in Figure 3c, the  $\text{SnO}_2$  electrode retains a good capacity of  $\sim 567 \text{ mAh g}^{-1}$  after 100 cycles in the ether electrolyte, but it only exhibits a lower capacity of  $\sim 499 \text{ mAh g}^{-1}$  in the carbonate electrolyte. Additionally, the average Coulombic efficiency in the ether

electrolyte (99.67%) surpasses that in the carbonate one (98.81%). To better summarize our results, we made a table in Supplementary Materials (Table S1) to compare the electrodes, electrolytes, capacities, and cycling performance.



**Figure 2.** Electrochemical characterizations of  $\text{SnO}_2$  in different voltage ranges. (a) CGD curves in the 0–2 V range; (b) GCD curves in the 0–1 V range; (c) the capacity and Coulombic efficiency comparison during cycling; (d) the scheme of the conversion–alloy reaction mechanism. The electrolyte is 1 M  $\text{LiPF}_6$ /EC-DEC (1:1 volume ratio, 10% FEC additives).



**Figure 3.** Electrochemical performance comparison of  $\text{SnO}_2$  in carbonate and ether electrolytes. (a) CGD curves in the 0–2 V range using the  $\text{LiPF}_6/\text{THF}+\text{m-THF}$  electrolyte; (b) rate performance comparison; (c) the cycling performance comparison; (d) the impedance comparison; (e) the cross-sectional SEM image of the cycled electrode in the ether electrolyte; (f) the cross-sectional SEM image of the cycled electrode in the conventional carbonate electrolyte.

To understand the performance differences, we conducted electrochemical impedance spectra (EIS) and ex situ SEM tests on the cycled battery. As shown in Figure 3d, these two batteries demonstrate a similar impedance response, with a semi-circle in the high-frequency region and a linear slope in the low-frequency region, corresponding to the charge-transfer resistance and ionic diffusion process, respectively [33–36]. After fitting the equivalent circuit, we find that the ether electrolyte exhibits a minimal charge-transfer resistance of 2.4 ohm, which is nearly 32 times lower than that of the carbonate electrolyte (80.6 ohm). Therefore, there is a much lower barrier for  $\text{Li}^+$  ions to cross the electrode–electrolyte interphase, which corroborates the observed high rate capability. Similar phenomena have also been observed in a recent work of  $\text{MnO}_2$  electrodes in aqueous ammonium-ion batteries [35].

Ex situ SEM reveals more information about electrode pulverization. As shown in Figure 3e, the cycled  $\text{SnO}_2$  electrode in the ether electrolyte is quite dense and compact, with a thickness of  $\sim 15 \mu\text{m}$  only. In comparison, the cycled electrode in the carbonate electrolyte is looser and more porous, with a larger thickness of  $\sim 25 \mu\text{m}$ . We reason that this difference may be related to the SEI formation. It has been reported that this ether electrolyte leads to the formation of an inorganic-rich lithium fluoride SEI on various anode materials [33], which is beneficial to maintaining the electrode integrity and alleviating the volume change. In contrast, it is known that the carbonate electrolyte has both inorganic and organic SEI components, which cannot effectively address the electrode volume change ratio. The comparison here clearly proves that electrolyte optimization is a feasible and promising approach to reinforce the  $\text{SnO}_2$  performance. Future studies will be carried out with  $\text{SnO}_2$  materials with novel composite structures to achieve even long-cycling performance.

#### 4. Conclusions

We demonstrated an effective approach to enhance the battery performance of  $\text{SnO}_2$  materials, wherein the voltage range of 0–1 V and an ether electrolyte were used concurrently. By limiting the voltage range, the conversion reaction can be circumvented, and the alloy reaction is facilitated, leading to improved cycling performance. When the carbonate is replaced with an ether electrolyte, the alloy reaction reversibility can be further enhanced,

owing to the reduced charge-transfer resistance and suppressed electrode pulverization. Consequently, pristine and commercial  $\text{SnO}_2$  delivers a promising battery performance, with a high capacity of  $\sim 650 \text{ mAh g}^{-1}$ , a high rate capability at  $1000 \text{ mA g}^{-1}$ , and stable cycling for 100 cycles. Our work provides an alternative understanding and insight into the use of  $\text{SnO}_2$  as high-capacity and cycle-stable anode materials.

**Supplementary Materials:** The following supporting information can be downloaded at <https://www.mdpi.com/article/10.3390/batteries10090334/s1>. Table S1: The performance comparison between this work and the literature.

**Author Contributions:** Conceptualization, X.W. and G.M.; investigation, J.F.F.G. and F.C.D.; data curation, J.F.F.G., F.C.D., S.C., V.D. and N.O.; writing—original draft preparation, J.F.F.G. and X.W.; writing—review and editing, X.W. and G.M.; supervision, X.W., G.M. and B.R.W.; funding acquisition, G.M. and X.W. All authors have read and agreed to the published version of the manuscript.

**Funding:** This work is financially supported by the NSF Center for the Advancement of Wearable Technologies (Grant No. 1849243), NASA EPSCoR (Grant No. 80NSSC22M0025), and NASA MIRO (Grant No. 80NSSC19M02346).

**Data Availability Statement:** The original contributions presented in the study are included in the article and Supplementary Materials, further inquiries can be directed to the corresponding authors.

**Conflicts of Interest:** The authors declare no conflicts of interest.

## References

- Yoshino, A. The birth of the lithium-ion battery. *Angew. Chem. Int. Ed.* **2012**, *51*, 5798–5800. [CrossRef] [PubMed]
- Choi, J.W.; Aurbach, D. Promise and reality of post-lithium-ion batteries with high energy densities. *Nat. Rev. Mater.* **2016**, *1*, 16013. [CrossRef]
- Goodenough, J.B.; Park, K.-S. The Li-ion rechargeable battery: A perspective. *J. Am. Chem. Soc.* **2013**, *135*, 1167–1176. [CrossRef]
- Xu, C.; Behrens, P.; Gasper, P.; Smith, K.; Hu, M.; Tukker, A.; Steubing, B. Electric vehicle batteries alone could satisfy short-term grid storage demand by as early as 2030. *Nat. Commun.* **2023**, *14*, 119. [CrossRef]
- Wu, F.; Maier, J.; Yu, Y. Guidelines and trends for next-generation rechargeable lithium and lithium-ion batteries. *Chem. Soc. Rev.* **2020**, *49*, 1569–1614. [CrossRef] [PubMed]
- Zhao, Y.; Fu, Y.; Meng, Y.; Wang, Z.; Liu, J.; Gong, X. Challenges and strategies of lithium-ion mass transfer in natural graphite anode. *Chem. Eng. J.* **2023**, *480*, 148047. [CrossRef]
- Mancini, M.; Martin, J.; Ruggeri, I.; Drewett, N.; Axmann, P.; Wohlfahrt-Mehrens, M. Enabling fast-charging lithium-ion battery anodes: Influence of spheroidization on natural graphite. *Batter. Supercaps* **2022**, *5*, e202200109. [CrossRef]
- Zhao, L.; Ding, B.; Qin, X.Y.; Wang, Z.; Lv, W.; He, Y.B.; Yang, Q.H.; Kang, F. Revisiting the roles of natural graphite in ongoing lithium-ion batteries. *Adv. Mater.* **2022**, *34*, 2106704. [CrossRef]
- Iwamura, S.; Nishihara, H.; Ono, Y.; Morito, H.; Yamane, H.; Nara, H.; Osaka, T.; Kyotani, T. Li-rich Li-Si alloy as a lithium-containing negative electrode material towards high energy lithium-ion batteries. *Sci. Rep.* **2015**, *5*, 8085. [CrossRef]
- Hamon, Y.; Brousse, T.; Jousse, F.; Topart, P.; Buvat, P.; Schleich, D.M. Aluminum negative electrode in lithium ion batteries. *J. Power Sources* **2001**, *97*, 185–187. [CrossRef]
- Crosnier, O.; Brousse, T.; Schleich, D. Tin based alloys for lithium ion batteries. *Ionics* **1999**, *5*, 311–315. [CrossRef]
- He, J.; Wei, Y.; Zhai, T.; Li, H. Antimony-based materials as promising anodes for rechargeable lithium-ion and sodium-ion batteries. *Mater. Chem. Front.* **2018**, *2*, 437–455. [CrossRef]
- Wang, M.; Zhang, F.; Lee, C.S.; Tang, Y. Low-cost metallic anode materials for high performance rechargeable batteries. *Adv. Energy Mater.* **2017**, *7*, 1700536. [CrossRef]
- Wang, M.; Chen, T.; Liao, T.; Zhang, X.; Zhu, B.; Tang, H.; Dai, C. Tin dioxide-based nanomaterials as anodes for lithium-ion batteries. *RSC Adv.* **2021**, *11*, 1200–1221. [CrossRef] [PubMed]
- Liu, M.; Liu, Y.; Zhang, Y.; Li, Y.; Zhang, P.; Yan, Y.; Liu, T. Octahedral tin dioxide nanocrystals anchored on vertically aligned carbon aerogels as high capacity anode materials for lithium-ion batteries. *Sci. Rep.* **2016**, *6*, 31496. [CrossRef]
- Heubner, C.; Liebmann, T.; Voigt, K.; Weiser, M.; Matthey, B.R.; Junker, N.; Lämmel, C.; Schneider, M.; Michaelis, A. Scalable fabrication of nanostructured tin oxide anodes for high-energy lithium-ion batteries. *ACS Appl. Mater. Interfaces* **2018**, *10*, 27019–27029. [CrossRef]
- Nowak, A.P. Composites of tin oxide and different carbonaceous materials as negative electrodes in lithium-ion batteries. *J. Solid State Electrochem.* **2018**, *22*, 2297–2304. [CrossRef]
- Zoller, F.; Böhm, D.; Bein, T.; Fattakhova-Rohlfing, D. Tin oxide based nanomaterials and their application as anodes in lithium-ion batteries and beyond. *ChemSusChem* **2019**, *12*, 4140–4159. [CrossRef]

19. Azam, M.A.; Safie, N.E.; Ahmad, A.S.; Yuza, N.A.; Zulkifli, N.S.A. Recent advances of silicon, carbon composites and tin oxide as new anode materials for lithium-ion battery: A comprehensive review. *J. Energy Storage* **2021**, *33*, 102096. [[CrossRef](#)]
20. Li, Z.; Wu, G.; Liu, D.; Wu, W.; Jiang, B.; Zheng, J.; Li, Y.; Li, J.; Wu, M. Graphene enhanced carbon-coated tin dioxide nanoparticles for lithium-ion secondary batteries. *J. Mater. Chem. A* **2014**, *2*, 7471–7477. [[CrossRef](#)]
21. Chen, Y.-C.; Chen, J.-M.; Huang, Y.-H.; Lee, Y.-R.; Shih, H.C. Size effect of tin oxide nanoparticles on high capacity lithium battery anode materials. *Surf. Coat. Technol.* **2007**, *202*, 1313–1318. [[CrossRef](#)]
22. Hong, Y.; Mao, W.; Hu, Q.; Chang, S.; Li, D.; Zhang, J.; Liu, G.; Ai, G. Nitrogen-doped carbon coated SnO<sub>2</sub> nanoparticles embedded in a hierarchical porous carbon framework for high-performance lithium-ion battery anodes. *J. Power Sources* **2019**, *428*, 44–52. [[CrossRef](#)]
23. Wang, Q.; Xu, J.; Shen, G.; Guo, Y.; Zhao, X.; Xia, Y.; Sun, H.; Hou, P.; Xie, W.; Xu, X. Large-scale carbon framework microbelts anchoring ultrafine SnO<sub>2</sub> nanoparticles with enhanced lithium storage properties. *Electrochim. Acta* **2019**, *297*, 879–887. [[CrossRef](#)]
24. Bagherian, S.; Zak, A.K. X-ray peak broadening and optical properties analysis of SnO<sub>2</sub> nanosheets prepared by sol-gel method. *Mater. Sci. Semicond. Process.* **2016**, *56*, 52–58. [[CrossRef](#)]
25. Wen, Z.; Zheng, F.; Liu, K. Synthesis of porous SnO<sub>2</sub> nanospheres and their application for lithium-ion battery. *Mater. Lett.* **2012**, *68*, 469–471. [[CrossRef](#)]
26. Li, H.; Su, Q.; Kang, J.; Huang, M.; Feng, M.; Feng, H.; Huang, P.; Du, G. Porous SnO<sub>2</sub> hollow microspheres as anodes for high-performance lithium ion battery. *Mater. Lett.* **2018**, *217*, 276–280. [[CrossRef](#)]
27. Rodriguez, J.R.; Hamann, H.J.; Mitchell, G.M.; Ortalan, V.; Gribble, D.; Xiong, B.; Pol, V.G.; Ramachandran, P.V. Interconnected Sn@SnO<sub>2</sub> nanoparticles as an anode material for lithium-ion batteries. *ACS Appl. Nano Mater.* **2023**, *6*, 11070–11076. [[CrossRef](#)]
28. Kilibarda, G.; Szabó, D.; Schlabach, S.; Winkler, V.; Bruns, M.; Hanemann, T. Investigation of the degradation of SnO<sub>2</sub> electrodes for use in Li-ion cells. *J. Power Sources* **2013**, *233*, 139–147. [[CrossRef](#)]
29. Jin, Y.; Kneusels, N.J.H.; Marbella, L.E.; Castillo-Martínez, E.; Magusin, P.C.; Weatherup, R.S.; Jonsson, E.; Liu, T.; Paul, S.; Grey, C.P. Understanding fluoroethylene carbonate and vinylene carbonate based electrolytes for Si anodes in lithium ion batteries with NMR spectroscopy. *J. Am. Chem. Soc.* **2018**, *140*, 9854–9867. [[CrossRef](#)]
30. Mirolo, M.; Wu, X.; Vaz, C.A.; Novák, P.; El Kazzi, M. Unveiling the Complex Redox Reactions of SnO<sub>2</sub> in Li-Ion Batteries Using Operando X-ray Photoelectron Spectroscopy and In Situ X-ray Absorption Spectroscopy. *ACS Appl. Mater. Interfaces* **2021**, *13*, 2547–2557. [[CrossRef](#)]
31. Ferraresi, G.; Villevieille, C.; Czekaj, I.; Horisberger, M.; Novák, P.; El Kazzi, M. SnO<sub>2</sub> model electrode cycled in Li-ion battery reveals the formation of Li<sub>2</sub>SnO<sub>3</sub> and Li<sub>8</sub>SnO<sub>6</sub> phases through conversion reactions. *ACS Appl. Mater. Interfaces* **2018**, *10*, 8712–8720. [[CrossRef](#)] [[PubMed](#)]
32. Chen, J.; Fan, X.; Li, Q.; Yang, H.; Khoshi, M.R.; Xu, Y.; Hwang, S.; Chen, L.; Ji, X.; Yang, C. Electrolyte design for LiF-rich solid-electrolyte interfaces to enable high-performance microsized alloy anodes for batteries. *Nat. Energy* **2020**, *5*, 386–397. [[CrossRef](#)]
33. Wang, C.; Appleby, A.J.; Little, F.E. Electrochemical study of the SnO<sub>2</sub> lithium-insertion anode using microperturbation techniques. *Solid State Ion.* **2002**, *147*, 13–22. [[CrossRef](#)]
34. Kong, Q.; Zhang, Q.; Yan, B.; Chen, J.; Chen, D.; Jiang, L.; Lan, T.; Zhang, C.; Yang, W.; He, S. N/O co-doped porous carbon synthesized by lewis acid salt activation for high rate performance supercapacitor. *J. Energy Storage* **2024**, *80*, 110322. [[CrossRef](#)]
35. Liu, Y.; Xiang, K.; Zhou, W.; Deng, W.; Zhu, H.; Chen, H. Investigations on tunnel-structure MnO<sub>2</sub> for utilization as a high-voltage and long-life cathode material in aqueous ammonium-ion and hybrid-ion batteries. *Small* **2024**, *20*, 2308741. [[CrossRef](#)]
36. Liu, J.; Li, Y.; Huang, X.; Ding, R.; Hu, Y.; Jiang, J.; Liao, L. Direct growth of SnO<sub>2</sub> nanorod array electrodes for lithium-ion batteries. *J. Mater. Chem.* **2009**, *19*, 1859–1864. [[CrossRef](#)]

**Disclaimer/Publisher’s Note:** The statements, opinions and data contained in all publications are solely those of the individual author(s) and contributor(s) and not of MDPI and/or the editor(s). MDPI and/or the editor(s) disclaim responsibility for any injury to people or property resulting from any ideas, methods, instructions or products referred to in the content.